Experimental and numerical study on Mode I and Mode II interfacial fracture toughness of co-cured steel-CFRP hybrid composites

Youqiang Yao, Pengcheng Shi, Mingda Chen, Gang Chen, Cong Gao, Philippe Boisse, Yingdan Zhu

Experimental and numerical study on Mode I and Mode II interfacial fracture toughness of co-cured steel-CFRP hybrid composites

Youqiang Yao [a,1], Pengcheng Shi [a,b,1], Mingda Chen [a], Gang Chen [a], Cong Gao [c], Philippe Boisse [d], Yingdan Zhu [a,b,*]

[a] *Zhejiang Provincial Key Laboratory of Robotics and Intelligent Manufacturing Equipment Technology, Ningbo Institute of Material Technology and Engineering, Chinese Academy of Sciences, Ningbo, 315201, China*
[b] *Center of Materials Science and Optoelectronics Engineering, University of Chinese Academy of Sciences, Beijing, 100049, China*
[c] *Changan Auto Global R&D Centre, Chongqing Changan Automobile Co. Ltd, Chongqing, China*
[d] *Université de Lyon, LaMCoS, CNRS, INSA-Lyon, F-69621, France*

Interfacial fracture toughness of co-cured steel-carbon fiber reinforced plastic (CFRP) hybrid composites were investigated in this paper. To illustrate the effect of the interlayer on the fracture toughness, steel-CFRP hybrid composites were prepared by different manufacturing processes based on steel surface treatment (abrasion or grit blasting) and adhesive-bonding process. The experimental results of double cantilever beam (DCB) tests and end notched flexure (ENF) tests demonstrate that, the Mode I and Mode II interfacial fracture toughness of the hybrid composites can be improved by using a grit blasting surface treatment on steel and introducing an adhesive layer at the steel/CFRP interface. The hybrid composites mainly show fiber/epoxy interfacial failure of CFRP under Mode I loading conditions, while it mostly exhibits adhesive failure of steel/CFRP interface under Mode II loading condition. Moreover, the interfacial tensile strengths of steel-CFRP hybrid composites are predicted by finite element analysis, and both experimental and numerical results confirm the improvement of interfacial fracture toughness.

1. Introduction

With fiber-metal laminates (FMLs) showing great application prospects in aerospace industries, metal-CFRP hybrid composites have also attracted great scientific and industrial interests in automotive structural applications [1,2]. Combining the outstanding high specific strength and fatigue resistance of fiber reinforced composites with the high bearing strength and impact resistance ductility of metal alloys, metal-CFRP hybrid composites possess lightweight and performance advantages that cannot be achieved by metals or advanced composites individually.

Nevertheless, the manufacturing of metal-CFRP hybrid composites still faces many challenges, such as weak bonding of heterogeneous material, residual stress caused by thermal expansion coefficient mismatch and galvanic corrosion caused by potential difference. The major defect is the relatively low bonding strength between metal substrate and CFRP laminate. Among a number of adhesion mechanisms, adsorption and mechanical interlock are well-known to be the dominant mechanisms that contribute to the adhesion strength of metal–polymer interfaces [3]. Thus, the adhesive optimization and surface treatment of metal substrate are two effective ways to improve bonding performance. On one hand, the adhesives should have good wettability with adherends. Relative to adhesives in a semi-solid state, liquid adhesives with lower surface tension than adherends are more likely to ensure uniform wetting of entire surfaces and improve molecular contacts between adherends, thereby increasing the joint strength [4]. On the other hand, to facilitate the bonding between metals and composites, many kinds of surface treatment methods for metal substrate have been developed including mechanical [5–10], chemical [11,12], electrochemical [13,14] treatment and so on. Among these methods, grit blasting is effective to achieve a coarse and high-energy metal surface. It has been widely used since it is non-polluting, easily adaptable, and

* Corresponding author. Zhejiang Provincial Key Laboratory of Robotics and Intelligent Manufacturing Equipment Technology, Ningbo Institute of Material Technology and Engineering, Chinese Academy of Sciences, Ningbo, 315201, China.
E-mail address: y.zhu@nimte.ac.cn (Y. Zhu).
[1] These authors contributed equally to this work and should be considered co-first authors.

Table 1
General characteristics of the matrix resin and epoxy adhesive.

	Type	Tensile strength (25 °C) [MPa]	Tensile modulus (25 °C) [MPa]	Elongation (25 °C) [%]	Poisson's coefficient
Matrix resin	Film	91	3500	5.2	0.34
Epoxy adhesive	Liquid	63	1907	7.5	0.34

economically viable [5–8]. Islam and Tong [10] indicated that, compared with needle gunning and wire brushed, grit blasting treated mild steel substrate possessed superior shear bond strength with glass epoxy prepreg composites even at different environment.

For metal-CFRP hybrid composites, interfacial fracture or delamination is one of the major failure modes, which may easily occur at the interface of the two dissimilar materials and result in severe degradation of overall structural strength [1,4]. In view of fracture mechanics, interfacial fracture toughness is an important parameter for measuring crack propagation resistance of the laminated composites [15]. Furthermore, the growth of interfacial cracks will be driven by the different crack tip loading conditions, where the Mode I and Mode II delamination patterns are often considered to be the most important failure modes [16]. Some studies have focus on the interfacial fracture toughness of the metal-composite adhesive joints [17–19]. Cortés and Cantwell [17] indicated that the Mg/CFRP sample offered a significantly higher fracture energy than the Mg/GFPP system, and the fracture energy for Mg/CFRP sample was slightly lower than that of plain CFRP. Reyes and Kang [18] mentioned that the critical strain energy release rate for metal-composite joint consisting of glass fiber reinforced polypropylene and aluminium significantly exceeded that of pure composite. Some studies have been carried out to improve the interlaminar fracture toughness of the metal-composite joints [20–22]. However, most of researches focus on aluminum-CFRP or magnesium-CFRP hybrid composites. The study on interfacial fracture toughness of steel-CFRP hybrid composites, especially detailed insight into the effect of surface treatment and adhesive on both Mode I and Mode II interfacial fracture toughness, has rarely been reported and is still required for further investigation.

In this study, the Mode I and Mode II interfacial fracture toughness of steel-CFRP hybrid composites prepared by different manufacturing process were investigated, which included the mechanical treatment applied to the steel surface and introduction of adhesive on the interface of the hybrid composites. Moreover, finite element analyses (FEA) were conducted to simulate fracture processes of steel-CFRP hybrid composites under Mode-I and Mode-II loading conditions and the interfacial tensile strength is successfully predicted which is difficult to obtained experimentally.

2. Material and methods

2.1. Materials

The steel substrates used in this study were hot stamping boron steel B1500HS from Baosteel Company in China, which was industrially processed to cold rolled steel plates with a thickness of 1.5 mm. A fast-curing prepreg (Y01-1 from Shenzhen No. 1 Company) with 200 g/m^2 in a twill fabric form was used to fabricate composite reinforcement. The matrix resin consisted of modified epoxy resin and modified imidazole microcapsules as curing agent. The epoxy number and average molecular weight of the matrix epoxy resin were about 0.5 eq/100g and 400 g/mol, respectively. The modified imidazole with 20% modifier was sealed in microcapsules. The epoxy adhesive used in this paper was SW-6 from Shanghai Huayi, a two-component adhesive that contained bisphenol A epoxy resin and modified phenolic amine as curing agent. The epoxy number and average molecular weight of the bisphenol A epoxy resin were about 0.4 eq/100g and 400 g/mol, respectively. The amine number of the curing agent was about 450 mgKOH/g. These two components were mixed accurately according to the weight ratio of 100 (bisphenol A epoxy resin) and 40 (curing agent) under the room temperature. The gelation time was about 2 h at 25 °C. The general physicochemical characteristics of the matrix resin and epoxy adhesive are provided by the manufacturer as shown in Table 1.

Table 2
Material properties of steel and CFRP.

Properties	Steel	CFRP
Modulus (GPa)	$E = 235$	$E_{11} = E_{22} = 48$, $E_{33} = 3.5$ $G_{12} = 3.66$, $G_{13} = G_{23} = 4.59$
Poisson's ratio	$\nu = 0.3$	$\nu_{12} = 0.37$, $\nu_{13} = \nu_{23} = 0.28$

Table 3
Sequence of manufacturing process for hybrid composites.

Code	Surface preparation	Forming process
HY-AB	Abrasion (#80 grit)	Co-cured without adhesive
HY-ABAD	Abrasion (#80 grit)	Co-cured with adhesive
HY-GB	Grit blasting (#60 grit)	Co-cured without adhesive
HY-GBAD	Grit blasting (#60 grit)	Co-cured with adhesive

The mechanical properties of steel and CFRP were experimentally tested in our previous study [23], as shown in Table 2.

2.2. Preparation of hybrid composites

The fabricated steel-CFRP hybrid composites consisted of a 1.50 mm thick steel layer and a 1.50 mm thick CFRP layer. As shown in Table 3, four types of steel-CFRP hybrid composites were prepared with different manufacturing processes.

2.2.1. Surface preparation of steel substrate

Abrasion or grit blasting has been commonly used to prepare the steel substrate to have rough, fresh and more reactive contact surface areas between the adhesive and substrate. Compared with abrasion, grit blasting is more effective to achieve a coarse and high-energy surface. These two mechanical treatment techniques were employed to prepare the surface of the steel substrate, abrasion (AB) and grit blasting (GB). Mechanical abrasion was carried out on the steel surface with an air sander, and the used sandpaper grit was 80. During grit blasting, 60 mesh white alundum (Al_2O_3) as blasting media was ejected onto the steel surface with a suction-fed, dry grit blasting machine. The pressure was 0.4 MPa with an approach angle of approximately 45° and a standard distance of 40 mm. After mechanical treatment, the steel substrates were degreased with acetone.

2.2.2. Forming process of hybrid composites

A co-curing compression molding process was used to prepare the hybrid composites. During the curing process, the CFRP prepregs with or without the adhesive were cured and bonded to the steel substrate in one-step. Two types of samples were prepared for comparison. One is the samples (HY-AB and HY-GB) without adhesive between steel and CFRP. For the other one, an epoxy adhesive SW-6 was introduced to the steel/CFRP interface (HY-ABAD and HY-GBAD). The mixed liquid adhesive was evenly applied to the surface of the steel substrate by a spray gun. The spread quantity was about 60 g/m^2 which was controlled by the spray cycles with constant spread quantity per second. To provide a starter pre-crack notch, Teflon film with 0.5 mm thickness was inserted

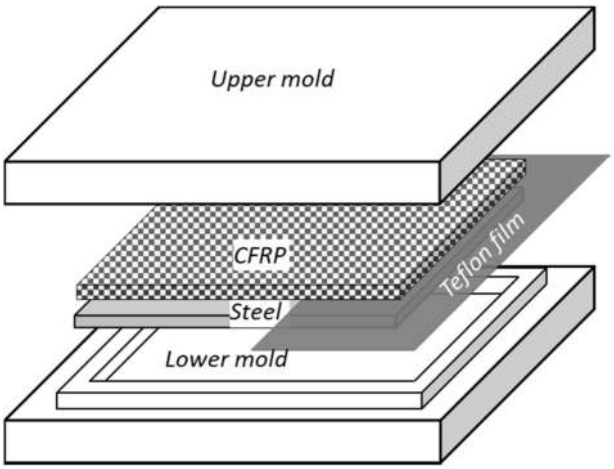

Fig. 1. Schematic of stacking arrangement of steel–CFRP composites in a mold.

into steel/CFRP interface at one edge of the hybrid composites. Then six layers of CFRP prepregs with consistent 0°/90° in fibers direction were placed on a steel substrate in a mold as shown in Fig. 1. The panels with a size of 290 mm × 190 mm were cured at 150 °C for 5 min in a hot-press machine. The heating rate was set to 5 °C/min and the pressure was kept at 2.5 MPa during the curing process. At last, the hybrid composites were removed from the mold after cooling to below 30 °C with a water cooling system.

Finally, four types of steel–CFRP hybrid composites were prepared. All of the test specimens were cut from the hybrid composites prepared above with a CNC Water Jet Cutting Machine possessing a machining accuracy of 0.1 mm. All specimens were stored at the standard laboratory atmosphere of 23 °C and 50–60% relative humidity for 24 h at least before testing, and all tests were conducted at the standard laboratory atmosphere. The average value for at least five specimens was taken as the test result for each case.

2.3. Double cantilever beam (DCB) test

According to ASTM D5528, a standard double cantilever beam (DCB) test was employed to evaluate Mode I interfacial fracture toughness. The DCB specimens were 135 mm in length, 25 mm in width with initial crack length of 50 mm. A pair of piano hinge tabs was bonded to the end of the specimens to introduce the load to the specimen during testing. To permit visual crack-tip location, the two sides of the specimen were painted white. The DCB tests were performed in an Instron 5985 test machine under a cross-head speed of 2 mm/min. Load versus displacement of each composite specimen was recorded to measure the interfacial fracture toughness G_{IC}. Location of the crack tip was tracked down regular intervals (every 5 mm) and recorded along with the applied loading and opening displacement at each measured crack extension.

According to the modified beam theory (MBT) introduced in ASTM D5528, the Mode I interfacial fracture toughness was determined as follows:

$$G_{IC} = \frac{3P\delta}{2b(a+\Delta)} \tag{1}$$

where P is applied load, δ is load point displacement, b is specimen width, a is delamination crack length, and Δ is the corrective factor for crack length which is determined experimentally by generating a least squares plot of the cube root of compliance, $C^{\frac{1}{3}}$, as a function of delamination crack length (a). The compliance, C, is the ratio of the load point displacement to the applied load, δ/P.

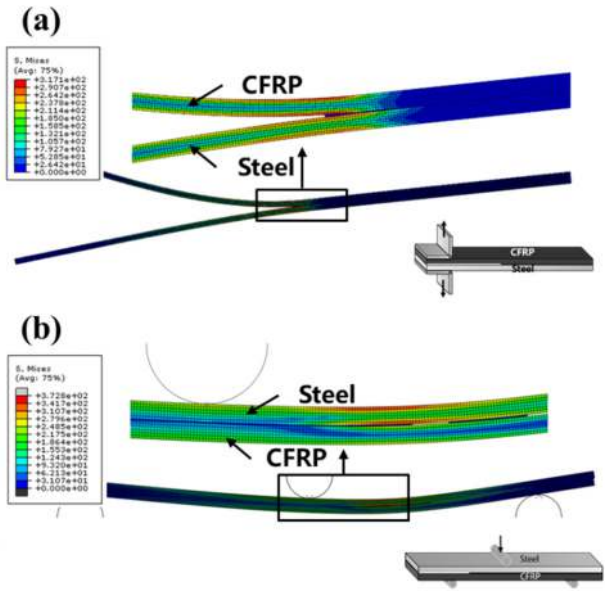

Fig. 2. FEA model of steel/CFRP hybrid composites for (a) DCB and (b) ENF tests.

2.4. End notched flexure (ENF) test

Mode II interfacial fracture toughness was characterized using an end notched flexure (ENF) test according to the ASTM D7905. The ENF specimens with length of 140 mm, width of 25 mm and initial crack length of 30 mm were cut from the fabricated hybrid composite plates. The ENF test was performed by a universal material testing machine (Instron 5985) under the cross-head speed of 2 mm/min at room temperature. Values of load and displacement were measured to calculate the Mode II interfacial fracture toughness G_{IIC}.

According to the compliance calibration method (CCM) introduced in ASTM D7905, the following expression was used to calculate G_{IIC}:

$$G_{IIC} = \frac{3mP_{Max}^2 a_0^2}{2B} \tag{2}$$

where P_{Max} is maximum load from the fracture test, a_0 is delamination crack length used in the fracture test (30 mm), B is specimen width, and m is the slope obtained from the regression analysis of the compliance, C, versus crack length cubed (a^3) of the form: $C = A + ma^3$.

2.5. Material characteristics

Finally, the detached surface morphology of the specimens after DCB and ENF tests were examined using a laser confocal scanning microscope (VK-X200K).

2.6. Finite element model

To simulate crack initiation and propagation processes during DCB and ENF tests, two-dimensional finite element analysis (FEA) models of hybrid composites were built with commercial software ABAQUS, as shown in Fig. 2. The models are made up with three main components: Steel substrate (CPE4I: 4-node bilinear plane strain elements), CFRP laminate (CPE4I), and Steel/CFRP interface (COH2D4: 4-node two-dimensional cohesive element.). The CFRP laminate was modeled as orthotropic material by effective properties of engineering constants. The detailed material parameters of steel substrate and CFRP laminates in simulations are shown in Table 2.

Cohesive elements are useful in modeling adhesives and bonded interfaces. A typical traction-separation response was adopted to define

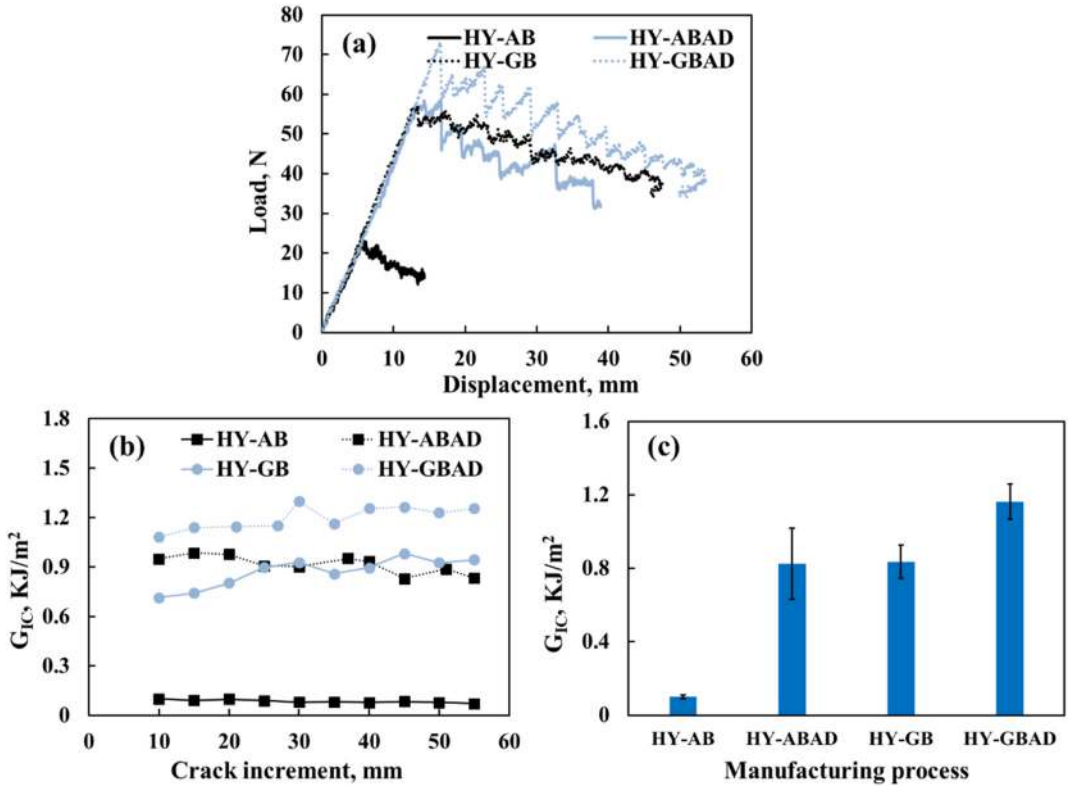

Fig. 3. (a) Typical load-displacement curve of DCB tests, (b) Calculated delamination resistance curves (R-curves) and (c) Mode-I interfacial fracture toughness (G_{IC}) for steel-CFRP hybrid composites with different manufacturing processes.

the progressive damage and failure in cohesive layers in ABAQUS/Explicit. The elastic behavior of the cohesive elements before damage initiation can be described as following [24]:

$$t_i = K_i \delta_i,\ i = n,\ s,\ t \tag{3}$$

where t, and δ represent the nominal traction stress vector and the corresponding separation, respectively, and n, s, and t represent the normal direction and two shear directions. The maximum nominal stress criterion was adopted to define the damage initiation which is shown below [24]:

$$max\left\{\frac{t_n}{t_n^0}, \frac{t_s}{t_s^0}, \frac{t_t}{t_t^0}\right\} = 1 \tag{4}$$

where t_i^0 (i = n, s, t) are the corresponding maximum traction in each direction. The delamination propagation was described by linear damage evolution based on fracture energy. For separate mode, traction-separation law mainly depends on the three parameters, i.e., initial stiffness (penalty stiffness, K), maximum traction (interfacial strength, N) and steady-state fracture energy (critical fracture energies, G).

3. Results and discussion

3.1. Mode I interfacial fracture toughness (DCB test)

Typical load-displacement curves of the hybrid composite specimens during DCB tests are shown in Fig. 3a. For each specimen, the load presents linear increase until a critical load is achieved, then the load gradually deceases with the delamination crack propagation. For the specimen with adhesive (HY-ABAD, HY-GBAD), the load fluctuates

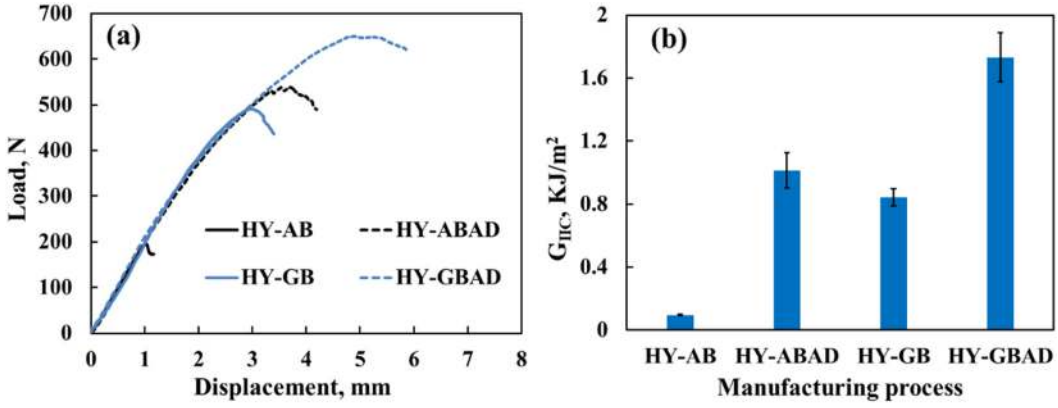

Fig. 4. (a) Typical load-displacement curve of ENF tests and (b) Calculated Mode-II fracture toughness (G_{IIC}) for steel-CFRP hybrid composites with different manufacturing process.

Table 4
Material properties of cohesive element in DCB model.

Specimen	E [MPa]	G_{IC} [kJ/m^2]	N_I [MPa]
HY-AB	3500	0.100	3
HY-ABAD	1907	0.825	8
HY-GB	3500	0.835	12
HY-GBAD	1907	1.161	20

greatly during decreasing. The calculated delamination resistance curves (R-curves) are shown in Fig. 3b. The calculated Mode-I fracture toughness (G_{IC}) is basically stable with delamination crack growth. The average fracture toughness of the four specimens is calculated and shown in Fig. 3c, and the standard deviations are indicated by the error bar. With grit blasting treatment on the steel surface, a great increase of G_{IC} for the HY-GB is observed compared with the HY-AB. For the specimen with adhesive, the HY-GBAD also shows higher G_{IC} than the HY-ABAD. This indicates that grit blasting treatment can enhance the interfacial fracture toughness of steel/CFRP composites effectively. With the introduction of adhesive into the steel/CFRP interface, the G_{IC} of the HY-ABAD gains highly improvement compared with that of HY-AB. Moreover, a further increase in the HY-GBAD demonstrates that combine grit blasting treatment on the steel surface and introduction of adhesive into the steel/CFRP interface, a superimposed improvement effect is produced.

3.2. Mode II interfacial fracture toughness (ENF test)

Fig. 4a shows typical load-displacement curves of ENF tests for steel-CFRP hybrid composites. For each specimen, the load initially presents linear increase, then shows a nonlinear increase after the yield point of the steel is reached. While the load reaches the peak value, drop occurs due to crack propagating at the critical load. The average Mode-II fracture toughness G_{IIC} for four specimens are calculated and shown in Fig. 4b. It shows similar tendency with the G_{IC}. Grit blasting treatment and introduction of adhesive can enhance the Mode II interfacial fracture toughness of steel/CFRP composites effectively, since the G_{IIC} for the HY-GB and the HY-ABAD are obviously higher than that of the HY-AB. The HY-GBAD which combines grit blasting treatment and introduction of adhesive possesses the highest G_{IIC}, which is much higher than those of HY-GB and HY-ABAD specimen. Thus, combine grit blasting treatment on the steel surface and introduction of adhesive into the steel/CFRP interface, a same superimposed improvement effect is produced on the Mode II interfacial fracture toughness of steel/CFRP composites.

3.3. Numerical simulation with the finite element method

As above, under Mode-I loading condition, the fracture toughness G_{IC} of steel/CFRP hybrid composites were obtained experimentally. The interfacial tensile strength N_I, which relates to the critical load for fracture, should be tested independently, such as a butt-joint test under tensile load. However, the butt-joint test for hybrid composites is difficult to carry out. Here, by matching the numerical load–displacement curves of DCB tests to the typical experimental ones, the interfacial tensile strengths N_I of four steel/CFRP hybrid composites were determined, similar to Li et al. [25]. Material properties of cohesive element are listed in Table 4. Note that G_{IC} is the experimental value obtained in Section 3.1, E is the elastic modulus of the adhesive, and the initial stiffness (K) of cohesive elements before crack propagation is automatically calculated by dividing the true thickness of the cohesive elements (0.01 mm). As illustrated in Fig. 5, comparing the four specimens with different G_{IC}, we can find that the maximum predicted loads show the same order of difference. The three numerical curves shown in each subplot are calculated by considering the predicated interfacial tensile strengths N_I and 20% higher and lower from that level (N_I, 1.2N_I, 0.8N_I). With a change of 20% in N_I, the maximum predicted load shows small difference, the same with the slope of the curve near maximum load. This indicates that the crack propagation is mainly driven by energy [26]. However, the interfacial tensile strengths N_I may be roughly deduced considering both the maximum load and the slope of the curve. As shown in Table 4, compare with 3 MPa for HY-AB, the N_I of HY-GB and HY-ABAD are enhanced to 8 MPa and 12 MPa, respectively. With grit blasting treatment and introduction of adhesive, the HY-GBAD shows lager strength with a value of 20 MPa. Therefore, both

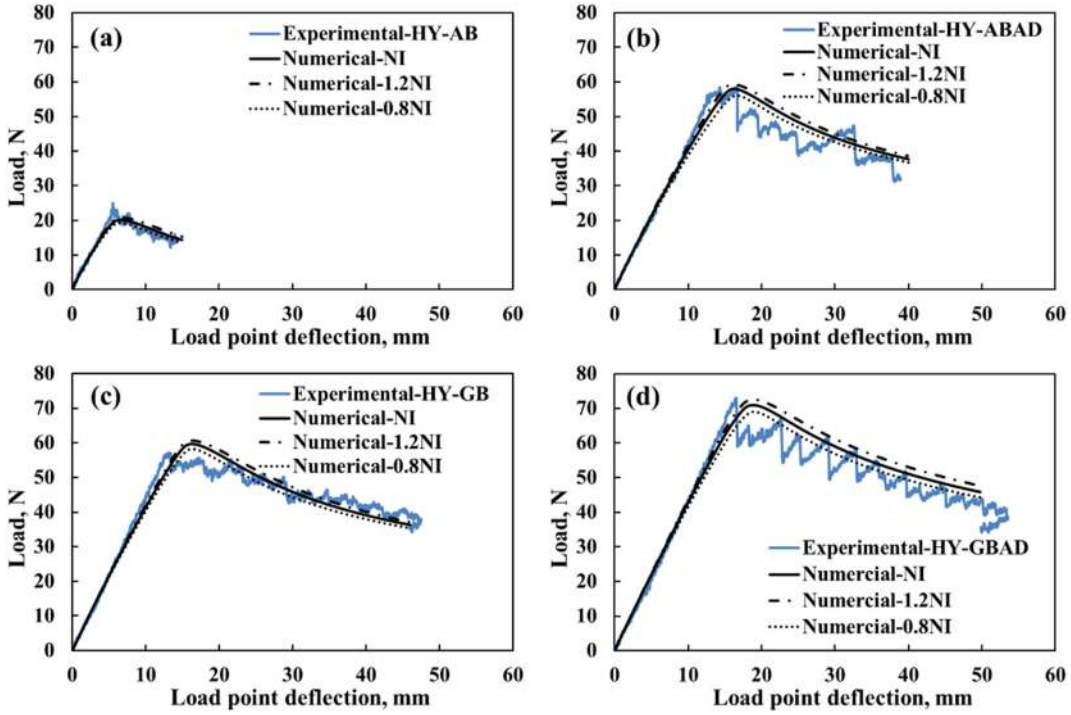

Fig. 5. Numerical and experimental load-displacement curves of DCB tests for steel-CFRP hybrid composites with different manufacturing processes.

Table 5

Material properties of cohesive element in ENF model.

Specimen	G [MPa]	G_{IIC} [kJ/m^2]	N_{II} [MPa]
HY-AB	1306	0.096	17.56
HY-ABAD	711	1.01	22.01
HY-GB	1306	0.843	18.68
HY-GBAD	711	1.733	23.69

numerical and experimental results confirm the improvement of the G_{IC} of steel/CFRP hybrid composites by grit blasting treatment and introduction of adhesive, and the improvement of the interfacial tensile strengths N_I of steel-CFRP hybrid composites which are roughly deduced by finite element analysis can be predicted.

For Mode-II loading condition, the interfacial shear strengths obtained from single-lap shear tests in our previous study [23] were used as N_{II}, as list in Table 5. G is the shear modulus of the adhesive. The comparison between numerical results of ENF tests and experimental ones (closest to the mean) is shown in Fig. 6. Since the experimental values of the interfacial shear strength N_{II} and G_{IIC} were directly used in the simulations, the good consistency between experimental and numerical results confirms the appropriateness of the ENF model.

Conclusively, the above results verify the appropriateness of the finite element models, and the appropriate values of each FEM parameters of the hybrid composites are clarified, which are helpful for the prediction of mechanical properties of complex structure. Moreover, both the numerical simulations and the experiments verify the improvement effect of grit blasting treatment and introduction of adhesive on the Mode-I and Mode-II interfacial mechanical properties of steel-CFRP hybrid composites.

3.4. Failure mode analysis

Fig. 7 presents the digital photographs of the detached surfaces after DCB tests. As shown in Fig. 7a, the failure of HY-AB mainly occurs at the steel/CFRP interface. The failure mode of the specimen is mainly adhesive failure between steel and epoxy. With grit blasting treatment, the HY-GB exhibits a mixed fracture mode, including fiber/epoxy interfacial failure and adhesive failure, since the CFRP can be observed on the detached steel surface with some matrix resin at where the fibers interweave, as shown in Fig. 7c. For the specimen with adhesive (HY-ABAD), the presence of adhesive cohesive failure can be confirmed with large area of residual adhesive on the detached steel surface, as shown in Fig. 7b. The specimen exhibits a mixed fracture mode, including adhesive cohesive failure and adhesive failure between adhesive and steel, accompanied with a degree of fiber/epoxy interfacial failure. With grit blasting treatment and introduction of adhesive, fiber/epoxy interfacial failure becomes the main failure mode of HY-GBAD. As shown in Fig. 7d, there is no steel surface exposed with CFRP and adhesive covered on it.

The failure modes of hybrid composites during ENF tests are much different with that during DCB tests. As shown in Fig. 8, all the four specimens mainly exhibit adhesive failure between adhesive and steel. Epoxy resin is observed on the grit blasted steel surface, indicating epoxy and adhesive cohesive failure occurs for HY-GB and HY-GBAD. The fiber/epoxy interfacial failure mode is rarely seen in Mode II loading conditions.

As we discussed in our previous study [23], grit blasting with the grit of 60 mesh would produce much rougher steel surfaces when compared with abrasion with sandpaper of 80 mesh. The surface roughness of the steel surface after abrasion and grit blasting are 1.6 mm and 10.0 mm, respectively. The thickness of the interphase region between steel and CFRP laminate (adhesive layer) was about 10 μm [23]. Rather than the thickness increase of the steel/CFRP interphase region and tougher property of the introduced adhesive, the steel/CFRP interfacial properties should mainly depend on the interface bonding of steel and adhesive. The good wetting of the adhesive on the steel substrate provides close contact between them and forms a good bond. The rougher surface generates by grit blasting significantly increase the interface area between steel and adhesive, which should contribute to the improvement of Mode I fracture toughness. The ravine features of steel surface can interlock with the epoxy, which may cause the cohesive failure of epoxy under shear loading condition and enhances the Mode II fracture

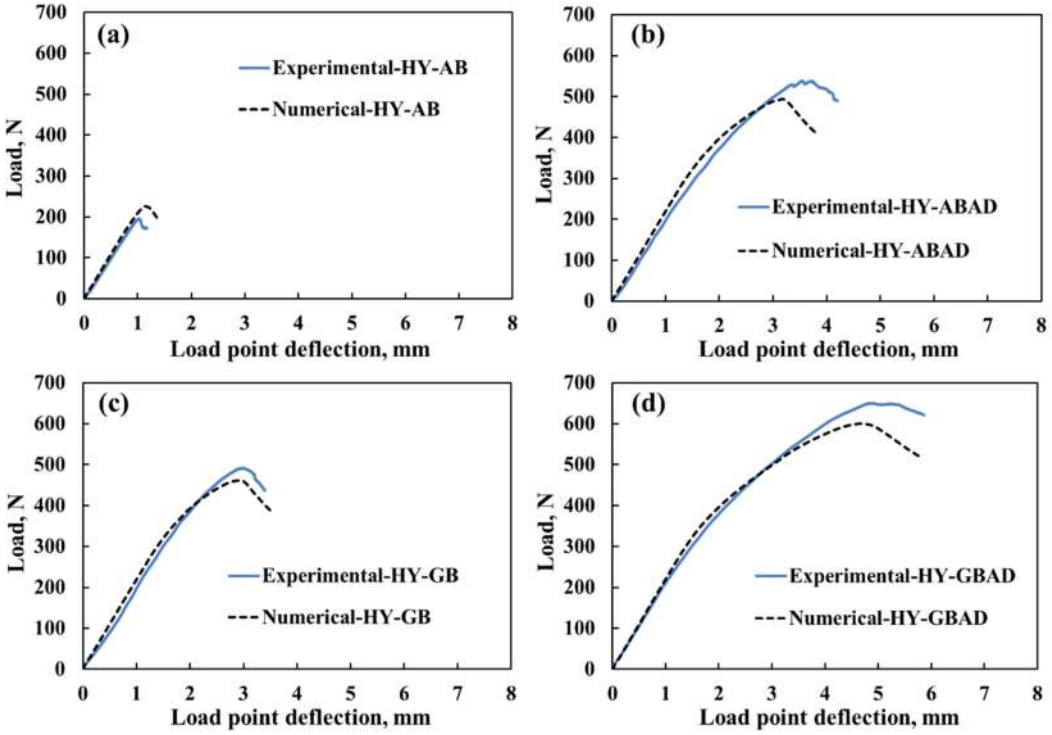

Fig. 6. Numerical and experimental load-displacement curves of ENF tests for steel-CFRP hybrid composites with different manufacturing process.

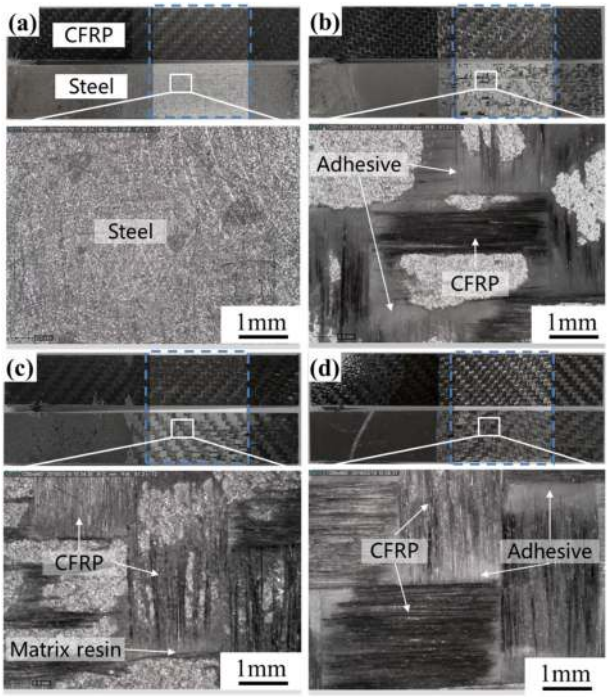

Fig. 7. Digital photographs of the detached surfaces after DCB tests for the steel-CFRP hybrid composites with different manufacturing process: (a) HY-AB, (b) HY-ABAD, (c) HY-GB, (d) HY-GBAD.

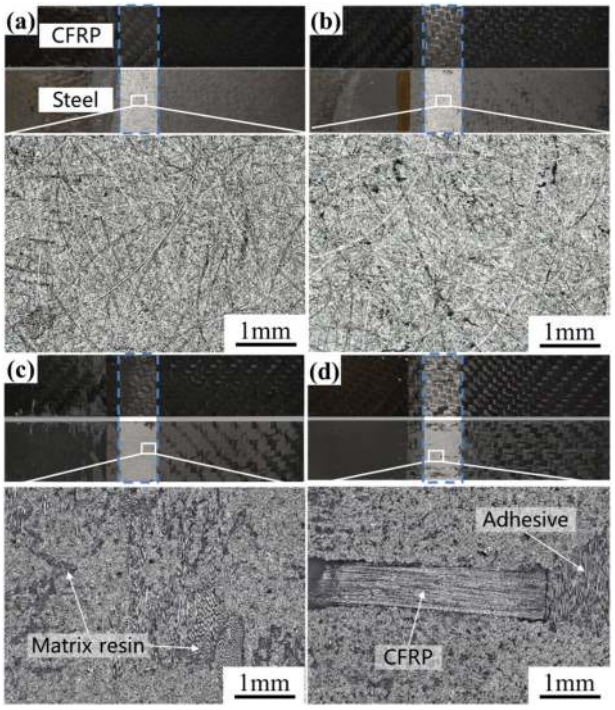

Fig. 8. Digital photographs of the detached surfaces after ENF tests for the steel-CFRP hybrid composites with different manufacturing process: (a) HY-AB, (b) HY-ABAD, (c) HY-GB, (d) HY-GBAD.

toughness through mechanical interlock.

In this work, the values of Mode II fracture toughness of hybrid composites are similar with that of Mode I fracture toughness. However, the failure modes of hybrid composites under Mode I and Mode II loading conditions show a big difference, which indicates that the failure modes in the hybrid composites are governed by different crack-tip loading conditions. With grit blasting treatment and introduction of adhesive, the main failure mode of HY-GBAD under Mode I loading condition is fiber/epoxy interfacial failure. This indicates that the Mode I interfacial fracture toughness of the steel/CFRP interface exceeds that of the plain CFRP. However, under Mode II loading condition, the HY-GBAD mainly exhibit adhesive failure between adhesive and steel, similar with other three specimens. There are still large gaps for the Mode II interfacial fracture toughness of the steel/CFRP interface compared with that of the plain CFRP. Some studies reported that for fiber reinforced polymers, there was a degree of difference between the G_{IC} and G_{IIC}, and the G_{IIC} was about twice higher than G_{IC} [17,22,27]. This may attribute to the bridging fibers connecting two opening surfaces for fiber reinforced polymers. Therefore, although the G_{IC} of the hybrid composites is higher than that of CFRP, the G_{IIC} of the hybrid composites is lower than that of CFRP, which results in that the steel/CFRP adhesive failure is the main failure mode of the hybrid composites under Mode II loading condition. Moreover, due to the structural asymmetry and material heterogeneity of hybrid composites, the interfacial fracture toughness from the DCB tests is in Mode I/II mixing at the crack tip [28–30]. The energy release rates in the initial crack lengths are mainly contributed by Mode I. With increasing the crack length, higher title angle of the specimen causes more contribution of Mode II on the fracture and increases the overall fracture toughness [29]. Since the G_{IC} has a great influence on the fitting of the load-displacement curves, the deduced interfacial tensile strength N_I may deviate from the real value. To eliminate the effect of shear loading at the crack front and assuring pure mode-I loading, the flexural rigidity of the CFRP should be equal to the flexural rigidity of the steel [31].

4. Conclusions

The paper studied the interfacial fracture toughness of co-cured steel-CFRP hybrid composites with the different manufacturing process and surface treatment. The results show that the Mode I and Mode II interfacial fracture toughness of the hybrid composites can be improved by using a grit blasting surface treatment on steel and introducing an adhesive layer at the steel/CFRP interface. The improved hybrid composites mainly show fiber/epoxy interfacial failure of CFRP under Mode I loading conditions, while for Mode II loading, it mostly exhibits adhesive failure of steel/CFRP interface. This may attribute to the higher G_{IC} and lower G_{IIC} of the hybrid composites, compared with the plain CFRP. Furthermore, the steel/CFRP interfacial tensile strength is predicted by finite element analysis, the good consistency between experimental and numerical results confirms the appropriateness of finite element models, and the appropriate values of each FEM parameters of the hybrid composites are clarified.

Acknowledgements

The authors gratefully acknowledge the financial support from the National Nature Sciences Foundation of China (U1809218, U1864211), Natural Science Foundation of Zhejiang Province (LQ20E030004), Ningbo Key Projects of Science and Technology Innovation 2025 Plan (2019B10118, 2020Z030, 2020Z116), Instrument Development Project of CAS (YJKYYQ20200029), and CAS President's International Fellowship Initiative (2020DE0011).

References

[1] Sinmazçelik T, Avcu E, Bora MÖ, Çoban O. A review: fibre metal laminates, background, bonding types and applied test methods. Mater Des 2011;32:3671–85. https://doi.org/10.1016/j.matdes.2011.03.011.
[2] Marsh G. Composites and metals – a marriage of convenience? Reinforc Plast 2014; 58:38–42. https://doi.org/10.1016/S0034-3617(14)70108-0.
[3] Kim W, Yun I, Lee J, Jung H. Evaluation of mechanical interlock effect on adhesion strength of polymer–metal interfaces using micro-patterned surface topography.

Int J Adhesion Adhes 2010;30:408–17. https://doi.org/10.1016/j.ijadhadh.2010.05.004.
[4] Pramanik A, Basak AK, Dong Y, Sarker PK, Uddin MS, Littlefair G, Dixit AR, Chattopadhyaya S. Joining of carbon fibre reinforced polymer (CFRP) composites and aluminium alloys – a review. Compos Part A-Appl S 2017;101:1–29. https://doi.org/10.1016/j.compositesa.2017.06.007.
[5] Rudawska A, Danczak I, Müller M, Valasek P. The effect of sandblasting on surface properties for adhesion. Int J Adhesion Adhes 2016;70:176–90. https://doi.org/10.1016/j.ijadhadh.2016.06.010.
[6] Poorna Chander K, Vashista M, Sabiruddin K, Paul S, Bandyopadhyay PP. Effects of grit blasting on surface properties of steel substrates. Mater Des 2009;30:2895–902. https://doi.org/10.1016/j.matdes.2009.01.014.
[7] Teng JG, Fernando D, Yu T, Zhao XL. Treatment of steel surfaces for effective adhesive bonding. In: Advances in FRP composites in civil engineering. Berlin, Heidelberg: Springer Berlin Heidelberg; 2011. https://doi.org/10.1007/978-3-642-17487-2_190.
[8] Islam MS, Tong L, Falzon PJ. Influence of metal surface preparation on its surface profile, contact angle, surface energy and adhesion with glass fibre prepreg. Int J Adhesion Adhes 2014;51:32–41. https://doi.org/10.1016/j.ijadhadh.2014.02.006.
[9] Pan Y, Wu G, Huang Z, Li M, Ji S, Zhang Z. Effect of surface roughness on interlaminar peel and shear strength of CFRP/Mg laminates. Int J Adhesion Adhes 2017;79:1–7. https://doi.org/10.1016/j.ijadhadh.2017.08.004.
[10] Islam MS, Tong L. Effects of hygrothermal and ambient humidity conditioning on shear strength of metal–GFRP single lap joints co-cured in and out of water. Int J Adhesion Adhes 2016;68:305–16. https://doi.org/10.1016/j.ijadhadh.2016.04.008.
[11] Dawood M, Rizkalla S. Environmental durability of a CFRP system for strengthening steel structures. Construct Build Mater 2010;24:1682–9. https://doi.org/10.1016/j.conbuildmat.2010.02.023.
[12] Ebnesajjad S. Chapter 7 - surface preparation of metals. In: Ebnesajjad S, editor. Surface treatment of materials for adhesive bonding. second ed. Oxford: William Andrew Publishing; 2014. p. 139–83.
[13] Baldan A. Adhesively-bonded joints and repairs in metallic alloys, polymers and composite materials: adhesives, adhesion theories and surface pretreatment. J Mater Sci 2004;39:1–49. https://doi.org/10.1023/B:JMSC.0000007726.58758.e4.
[14] Teng JG, Yu T, Fernando D. Strengthening of steel structures with fiber-reinforced polymer composites. J Constr Steel Res 2012;78:131–43. https://doi.org/10.1016/j.jcsr.2012.06.011.
[15] Morita H, Adachi T, Tateishi Y, Matsumoto H. Characterization of impact damage resistance of CF/PEEK and CF/toughened epoxy laminates under low and high velocity impact tests. J Reinforc Plast Compos 1997;16:131–43. https://doi.org/10.1177/073168449701600203.
[16] Boon YD, Joshi SC. A review of methods for improving interlaminar interfaces and fracture toughness of laminated composites. Mater Today Commun 2020;22:100830. https://doi.org/10.1016/j.mtcomm.2019.100830.
[17] Cortés P, Cantwell WJ. The fracture properties of a fibre–metal laminate based on magnesium alloy. Compos B Eng 2005;37:163–70. https://doi.org/10.1016/j.compositesb.2005.06.002.
[18] Reyes G, Kang H. Mechanical behavior of lightweight thermoplastic fiber–metal laminates. J Mater Process Technol 2007;186:284–90. https://doi.org/10.1016/j.jmatprotec.2006.12.050.
[19] Abdullah MR, Prawoto Y, Cantwell WJ. Interfacial fracture of the fibre-metal laminates based on fibre reinforced thermoplastics. Mater Des 2015;66:446–52. https://doi.org/10.1016/j.matdes.2014.03.058.
[20] Ning H, Weng S, Hu N, Yan C, Liu J, Yao J, Liu Y, Peng X, Fu S, Zhang J. Mode-II interlaminar fracture toughness of GFRP/Al laminates improved by surface modified VGCF interleaves. Compos B Eng 2017;114:365–72. https://doi.org/10.1016/j.compositesb.2017.02.022.
[21] Pan Y, Wu X, Huang Z, Wu G, Sun S, Ye H, Zhang Z. A new approach to enhancing interlaminar strength and galvanic corrosion resistance of CFRP/Mg laminates. Compos Part A-Appl S 2018;105:78–86. https://doi.org/10.1016/j.compositesa.2017.11.009.
[22] Arai M, Noro Y, Sugimoto K-i, Endo M. Mode I and mode II interlaminar fracture toughness of CFRP laminates toughened by carbon nanofiber interlayer. Compos Sci Technol 2008;68:516–25. https://doi.org/10.1016/j.compscitech.2007.06.007.
[23] Yao Y, Shi P, Qi S, Yan C, Chen G, Liu D, Zhu Y, Herrmann A. Manufacturing and mechanical properties of steel-CFRP hybrid composites. J Compos Mater 2020;54:3673–82. https://doi.org/10.1177/0021998320918287.
[24] Abaqus/CAE user's manual DS SIMULIA 2016 providence Rhode Island. http://130.149.89.49:2080/v6.14/pdf_books/CAE.pdf.
[25] Li Y, Hori N, Arai M, Hu N, Liu Y, Fukunaga H. Improvement of interlaminar mechanical properties of CFRP laminates using VGCF. Compos Part A-Appl S 2009;40:2004–12. https://doi.org/10.1016/j.compositesa.2009.09.002.
[26] Anyfantis KN. On the failure analysis of bondlines: stress or energy based fracture criteria? Eng Fract Mech 2014;126:108–25. https://doi.org/10.1016/j.engfracmech.2014.04.024.
[27] Reyes VG, Cantwell WJ. The mechanical properties of fibre-metal laminates based on glass fibre reinforced polypropylene. Compos Sci Technol 2000;60:1085–94. https://doi.org/10.1016/S0266-3538(00)00002-6.
[28] Hua X, Li H, Lu Y, Chen Y, Qiu L, Tao J. Interlaminar fracture toughness of GLARE laminates based on asymmetric double cantilever beam (ADCB). Compos B Eng 2019;163:175–84. https://doi.org/10.1016/j.compositesb.2018.11.040.
[29] Zamani Zakaria A, Shelesh-nezhad K, Navid Chakherlou T, Olad A. Effects of aluminum surface treatments on the interfacial fracture toughness of carbon-fiber aluminum laminates. Eng Fract Mech 2017;172:139–51. https://doi.org/10.1016/j.engfracmech.2017.01.004.
[30] Sundararaman V, Davidson BD. An unsymmetric double cantilever beam test for interfacial fracture toughness determination. Int J Solid Struct 1997;34:799–817. https://doi.org/10.1016/S0020-7683(96)00055-8.
[31] Wang W, De Freitas ST, Poulis JA, Zarouchas D. A review of experimental and theoretical fracture characterization of bi-material bonded joints. Compos B Eng 2021;206:108537. https://doi.org/10.1016/j.compositesb.2020.108537.